

A Wave Packet Approach to Resonant Scattering

A. M. Michalik and F. Marsiglio

Department of Physics, University of Alberta, Edmonton, Alberta, Canada, T6G 2E1

(Dated: November 1, 2022)

Resonant transmission occurs when constructive interference results in the complete passage of an incoming wave through an array of barriers. In this paper we explore such a scenario with one dimensional models. We adopt wave packets with finite width to illustrate the deterioration of resonance with decreasing wave packet width, and suggest an approximate wave function for the transmitted and reflected components, derived from aspects of both the wave packet and plane wave approaches. A comparison with exact numerical calculations shows excellent agreement, and provides insight into the scattering process.

I. INTRODUCTION

Scattering experiments are one of the most effective ways of probing matter. Going back into the distant past, physicists have been throwing projectiles at objects to learn something about the projectile, the object, or the interaction between the two. For example, Newton used a prism to learn about the properties of the projectile (light), and Young used a double slit experiment for the same purpose.

Over the course of the last century, however, scattering experiments have been associated more with learning about the object. A classic example is the series of alpha scattering experiments by Geiger and Marsden¹ with guidance from Rutherford. In this experiment, alpha particles were used to learn about the inner structure of the atom. Modern particle accelerators use higher energy particle beams to probe the internal structure of the nucleus. Larger scale targets, be they molecules or solids, utilize the same principle with using X-rays or neutron beams. In each case the incoming energy can be varied, and the scattering profile can be measured as a function of angle and outgoing energy. These are all three-dimensional problems, and our understanding of them is well developed partly because we focus on the simplified scenario where the incoming and outgoing projectiles are well-described by a plane wave. In this paper we move beyond the plane wave approximation and consider incoming and outgoing wave packets. To keep things relatively simple we follow the traditional procedure used in the plane wave approach by first restricting ourselves to one dimension. The two- or three-dimensional case is considerably more complicated and is beyond the scope of this article.

Several recent descriptions of one-dimensional quantum scattering have emphasized the wave packet approach.²⁻⁷ All of this work has espoused the conceptual advantages of real-time wave packet scattering over the stationary plane wave approximation found in standard undergraduate quantum texts, and in addition, two of these groups have adopted a lattice approach. For example, Ref. 5 emphasized the differences with the continuum approach and focused on narrow wave packets. In Ref. 6 one simulation focused on a dimer (two-impurity) barrier

where resonant transmission was known to take place and modeled the time-dependent scattering interference. Our group^{2,3,6} has exploited a remarkable feature: the lack of spreading for reasonably broad Gaussian wave packets on a lattice for certain wave vectors. Such wave packets maintain their qualitative characteristics during propagation and, therefore, make the effects of the scattering process clearer.

In this work, we want to do two things. First, we will generalize the possibilities for resonant transmission by considering any number of barriers. Various aspects of this problem have already appeared in the literature,^{11,12} with some variation of what we consider here, so we will merely provide a brief overview of the theory. More specifically, we consider scattering from a periodic array of N identical impurities/barriers, each spaced m lattice sites apart. This problem is likely to be more familiar to the reader in the continuum limit, and has been addressed through the transfer matrix formalism in Ref. 13. The tight-binding limit of various models of this problem on a lattice has also been treated in Refs. 2, 3, and 9. For completeness, a derivation is presented in the online Supplementary Material. The result of this derivation is that, given a barrier configuration consisting of N impurity potentials, each with strength V , spaced m lattice spacings apart, then, for a particular dispersion relation, there will exist a number of plane waves with fixed wave vector that will yield unit transmission and zero reflectance.

However, there is a conceptual shortcoming with a time-independent plane wave approach: it does not give a complete qualitative understanding of the scattering process, especially during resonant transmission. From a plane wave description, we can calculate the transmission of reflection coefficients, but the components themselves are always plane waves before and after the scattering process. At resonance, the reflected component is exactly zero. Using a Gaussian wave packet that retains its shape under propagation and nonresonant scattering, we can show that the reflected wave packet profile at resonance is non-zero, contrary to the wave packet description. It is also no longer Gaussian. This reflected shape profile is derivable from a plane wave description of sufficiently broad wave packets.

Therefore our second goal in this paper is to study how the scattering profile changes when a Gaussian wave-

packet with real-space width $\alpha < \infty$ is used (as $\alpha \rightarrow \infty$ we approach the plane wave description). In this case, even at resonance, the transmission will be less than unity and a reflected portion will appear. We can study the dependence of the reflected portion on the wave packet width. Numerically we find a very peculiar shape for the reflected packet, while the transmitted portion remains essentially Gaussian. In addition we derive a closed approximate analytical formula which works remarkably well, both in describing the reflection and transmission, and in giving the detailed form of the scattered wave packet profile. We will examine the validity and limitations of this approximation by comparing it with exact numerical solutions. It will be clear that when barriers with extended spatial structure are used, increasingly wide wave packets are required to recover the plane wave results.

As mentioned earlier, when the scattering problem is defined on a lattice, wave packets with a specific centroid wave vector do not spread with time,^{2,3,6} unlike the continuum case. The lattice model requires the use of the tight-binding formalism (see online Supplementary Materials for technical details), but allows for a much clearer description of the scattering process. Senior undergraduate students should be able to understand the content of this paper and follow the required numerical work. These students should also be able to reproduce most of the paper's content as a long-term project, assuming they have completed a numerical methods prerequisite course.

II. PLANE-WAVE SCATTERING ON A LATTICE FROM A FINITE PERIODIC ARRAY

Following Ref. 6 we adopt as a basis the site representation, where, using bra-ket notation, each (orthonormal) basis state, $|\ell\rangle \equiv c_\ell^\dagger|0\rangle$, represents a particle at position $x_\ell \equiv \ell a$, with a the lattice spacing and ℓ an integer. Here, c_ℓ^\dagger (c_ℓ) represents the creation (annihilation) operator for a particle at site ℓ , and $|0\rangle$ is the vacuum state, i.e. the empty lattice state, and ℓ is one of L lattice sites. In principle, $L \rightarrow \infty$ while, in practice, L is some large integer. We also adopt periodic boundary conditions.

Initially we imagine a plane wave impinging from the left; without barriers this wave would continue unimpeded towards the right. Propagation consists of ‘‘hops’’ from one site to another, and for simplicity we consider here nearest-neighbour hops only. This part of the Hamiltonian constitutes the kinetic energy part, denoted by H_0 , and is written as

$$H_0 = -t_0 \sum_{\ell} \left(c_\ell^\dagger c_{\ell+1} + c_{\ell+1}^\dagger c_\ell \right), \quad (1)$$

where t_0 is the hopping amplitude. The eigenstates of this Hamiltonian alone are Bloch states, with wave vector $ka \equiv 2\pi n/L$ and n an integer with domain $-L/2 < n \leq$

$L/2$. These eigenstates are given by

$$c_k^\dagger = \frac{1}{\sqrt{L}} \sum_{\ell'} e^{ik\ell'} c_{\ell'}^\dagger, \quad (2)$$

where the summation is over all sites. Application of the hopping Hamiltonian, Eq. 1, to this state confirms that it is an eigenstate with eigenvalue $E_k = -2t_0 \cos(ka)$.

In general there is a finite barrier region, starting at site I_1 . This barrier consists of N one-body potentials arranged periodically with a barrier lattice spacing of ma , where m is a positive integer. The N barriers are localized at sites $I_1, I_2 \equiv I_1 + m, I_3 \equiv I_1 + 2m, \dots, I_N \equiv I_1 + (N-1)m$, and the Hamiltonian describing the interaction with the incoming particle (described for now as a plane wave) is

$$H_V = \sum_{\ell \in \mathcal{I}} V_\ell c_\ell^\dagger c_\ell = V \sum_{\ell \in \mathcal{I}} c_\ell^\dagger c_\ell, \quad (3)$$

where the second equality follows since we assume all barrier strengths to be equal (hence the barrier has periodic structure). Since the barrier is finite it has a total width given by

$$w_B \equiv (N-1)ma. \quad (4)$$

A presumed solution for the wave function,

$$|\psi\rangle = \sum_{\ell=1}^L a_\ell |\ell\rangle \equiv \sum_{\ell=1}^L a_\ell c_\ell^\dagger |0\rangle, \quad (5)$$

can be substituted into the Schrödinger equation, $H|\psi\rangle = E|\psi\rangle$. This procedure is described in the online Supplementary Materials, where appropriate plane wave solutions are assumed to the left and right of the barrier region (as is done in textbooks in the continuum limit). Using the transfer matrix formalism (briefly reviewed in the online Supplementary Material), we ultimately derive the simple result⁹ for the transmission T on a lattice with spacing a , of a plane wave with wave-vector k , through N barriers, each m lattice spacings apart, and each with strength V ,

$$T = \frac{1}{1 + [v_k U_{N-1}(h_k)]^2}, \quad (6)$$

where

$$v_k \equiv \frac{V}{2t_0 \sin(ka)}, \quad (7)$$

$$h_k \equiv \cos(kma) + v_k \sin(kma), \quad (8)$$

and $U_n(x)$ is the n^{th} Chebyshev polynomial of the second kind (in x), with properties as described in the online Supplementary Material D. The reflection probability can easily be derived since the transmission and reflection probabilities have to sum to unity, and therefore

$$R = 1 - T = \frac{[v_k U_{N-1}(h_k)]^2}{1 + [v_k U_{N-1}(h_k)]^2} \equiv \frac{f^2(k)}{1 + f^2(k)}, \quad (9)$$

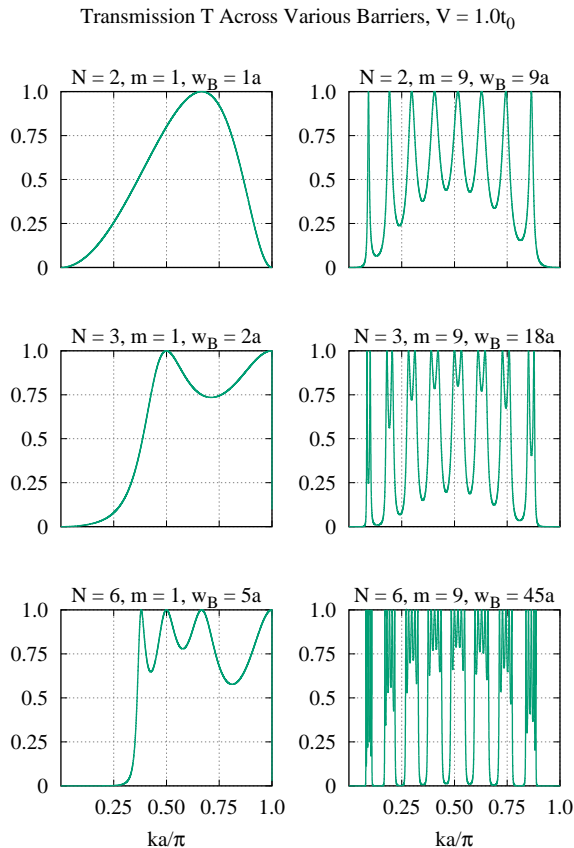


FIG. 1. Transmission T vs. ka/π , across barriers with strength $V = 1.0t_0$ and various values of N , m and w_B as indicated above the various panels. Only positive values of k , with range $0 < ka/\pi < 1$, are plotted. The energy, $E_k = -2t_0 \cos(ka)$, increases monotonically from $-2t_0$ to $+2t_0$ over this range. Note the many instances of resonant transmission ($T = 1$). As V changes, the value of the wave vector where resonance will occur will change according to Eq. (10). Note that $ka = \pi/2$ is special for wave packet propagation, as spreading with time is limited at this wave vector, given the nearest-neighbor hopping model we have adopted. Amongst these six examples unit transmission is clearly seen to occur at this wave vector for all four cases beyond the first row ($N = 2$).

where for convenience we define $f(k) \equiv v_k U_{N-1}(h_k)$. These quantities are further discussed in the online Supplementary Material, along with the amplitudes $\rho(k)$ and $\tau(k)$, where $R \equiv |\rho|^2$ and $T \equiv |\tau|^2$. A version of Eq. (6) applicable to free electrons in the continuum seems to have been first derived in Ref. 11 for an array of δ -functions, and in Ref. 12 for a more general array; see references therein for earlier related work. See also Ref. 13 for further discussion on transmission in the continuum limit.

From the general transmission relation Eq. (6) we can calculate the barrier parameters for which unit transmission (resonance) occurs. Unit transmission occurs obviously for $V = 0$, i.e. no impurities, or when $U_{N-1}(h_k) =$

0 for a non-zero value of V . The non-trivial resonant condition is therefore

$$U_{N-1}(h_k) = 0, \quad (10)$$

where $h_k = (h_k^{(n)})_{root}^{N-1}$ is the n^{th} root of the $N-1$ Chebyshev polynomial, and the barrier parameters are chosen such that

$$(h_k^{(n)})_{root}^{N-1} = \cos(kma) + \frac{V \sin(kma)}{2t_0 \sin(ka)} \quad (11)$$

is satisfied.

For a single impurity, $N = 1$, only the trivial solution exists since $U_{N-1}^2(h_k) = U_0^2(h_k) = 1$ for all k , hence no resonance can occur with a single impurity. For a barrier configuration with $N \geq 2$ impurities, a potential V and wave vector k can always be found that satisfy Eq. (11) for a given impurity lattice spacing ma and number of impurities N .

Examples of transmission across different barriers, of potential strength $V = 1.0t_0$, are shown in Fig. 1 for selected values of N and m . It is clear from Eqs. (10)-(11), and as shown in Fig. 1, that resonant transmission ($T = 1$) is possible at many different values of the wave vector k , and the number of these resonant points increases with increasing barrier parameters N and m . Plots similar to Fig. 1 can be found in many references, for example Refs. 2, 3, 9, 11–13. These plots all convey the idea that resonant transmission is possible at certain energies (i.e. values of wave vector k), whose values depend on the specific parameters and details of the barriers. Students are taught that this is due to constructive interference effects for a plane wave description. How is the resonant transmission and (lack of) reflection altered when wave packets are used? Before addressing this question we briefly review how wave packets are constructed on a lattice.

III. THE WAVE PACKET DESCRIPTION

As mentioned in the introduction, there are many reasons to favor a wave packet description of the incoming particle, not least of which is that it allows a time-dependent evolution of the actual scattering event. We follow previous prescriptions for such a wave packet description^{2,3,6} by constructing a set of eigenstates for the Hamiltonian that is the sum of Eq. (1) and Eq. (3). Then the eigenstates can be written formally as

$$|n\rangle = \sum_{\ell} a_{\ell}^{(n)} c_{\ell}^{\dagger} |0\rangle \quad (12)$$

where $a_{\ell}^{(n)}$ are the eigenvector coefficients for the n^{th} eigenstate with eigenvalue ϵ_n , both obtained through numerical matrix diagonalization. It follows that the time-dependent wave packet is

$$|\psi(t)\rangle = \sum_{n=1}^L |n\rangle \langle n|\psi(0)\rangle e^{-i\epsilon_n t/\hbar}, \quad (13)$$

and the site-dependent wave function is given by $\langle \ell | \psi(t) \rangle$ to obtain

$$\psi(x_\ell, t) = \sum_{n=1}^L a_\ell^{(n)} \langle n | \psi(0) \rangle e^{-i\epsilon_n t/\hbar}, \quad (14)$$

where $a_\ell^{(n)}$ represents the ℓ^{th} element of the n^{th} eigenvector and $\langle n | \psi(0) \rangle = \sum_\ell [a_\ell^{(n)}]^* \phi(x_\ell)$, with the initial wave function given by

$$|\psi(t=0)\rangle = \sum_\ell \phi(x_\ell) |\ell\rangle, \quad (15)$$

and the initial profile is described by a Gaussian,

$$\phi(x_\ell) = \frac{1}{(2\pi\alpha^2)^{1/4}} e^{-\frac{1}{4}(x_\ell - x_0)^2/\alpha^2 + ik_0(x_\ell - x_0)}. \quad (16)$$

Here x_0 and k_0 are the mean position and mean wave vector of the wave packet, respectively, and α is the initial uncertainty in position (i.e. spread) of the wave packet. Once the eigenvalues and eigenvectors are calculated, a straightforward summation in Eq. (14) produces the wave function profile at any time thereafter.

In fact this summation is relatively straightforward to implement in an empty lattice (i.e. no barriers whatsoever). It would give the novice student both the practice required to tackle the problem with a barrier in place and the satisfaction of seeing a moving wave packet in motion [given by Eq. (14)] that also does not spread if $k_0 a = \pi/2$ is used for the mean wave vector.¹⁵

One of the primary reasons for using wave packets specifically defined on a lattice is that a wave vector can be found for which the intrinsic spreading is essentially eliminated. A very good approximation to the time-dependent wave function, previously derived in Refs. 2 and 3 for an empty lattice, is given by

$$\begin{aligned} \psi(x_\ell, t) = & \left(\frac{\alpha^2}{2\pi}\right)^{1/4} \frac{e^{ik_0(x_\ell - x_s) - iE_{k_0} t/\hbar}}{\sqrt{\alpha^2 + itE''_{k_0}/(2\hbar)}} \\ & \times \exp\left[-\frac{1}{4} \frac{(x_\ell - x_s - tE'_{k_0}/\hbar)}{\alpha^2 + itE''_{k_0}/(2\hbar)}\right] \end{aligned} \quad (17)$$

where E'_{k_0} and E''_{k_0} refer to the first and second derivatives of the dispersion relation E_k with respect to wave vector k , evaluated at k_0 . For nearest-neighbour hopping the dispersion relation is given by $E_k = -2t_0 \cos(ka)$. It follows in this case that the spread of the wave packet, as a function of time, will be constant for $k_0 a = \pi/2$, and is given by the initial width α .

As an example, in Fig. 2(a) we show a sequence of snapshots of a travelling wave packet, with $k_0 a = \pi/2$, that encounters two ($N = 2$) barriers set side-by-side ($m = 1$) at $x_\ell = 1500a$ and $x_\ell = 1501a$. No spreading is predicted to take place on an empty lattice. Two snapshots ($t = 0$ and $t = 250\hbar/t_0$) are shown before scattering takes place

and two snapshots ($t = 750\hbar/t_0$ and $t = 1000\hbar/t_0$) are shown for times after scattering. “Before” and “after” here are loosely defined and are meant to signify that the wave packet profile is entirely to the left and right of the barrier region, respectively, as viewed by eye in such a figure. Since a Gaussian has tails this is necessarily a loose definition. The middle panel, showing the scattering event as the wave packet strikes the barrier, displays considerable disruption in the wave packet. More detailed descriptions of these transient phenomena can be found in the simulations in Ref. 6. It should be clear from the two times chosen before and after the scattering, that no spreading takes place, as the peak heights remain the same. In particular it is true that no spreading takes place in either the transmitted or reflected wave packets. A sizable reflectance takes place in Fig. 2(a) of approximately 20%. From the curve shown in Fig. 1 ($N = 2$, $m = 1$) it is clear that the transmission is indeed expected to be approximately 80% for this barrier configuration.

In contrast, in Fig. 2(b) we show snapshots of a wave packet with $k_0 a = 2\pi/3$, for which spreading is anticipated based on Eq. (17). Referring back to Fig. 1 ($N = 2$, $m = 1$), we see that unit transmission is anticipated for this wave vector. Sure enough, inspection of Fig. 2(b) shows a small decrease in amplitude of the wave packet due to spreading as time progresses. Notice that the wave packet travels a little more slowly than the one in Fig. 2(a) since the group velocity, $v_{\text{gr}}(k) \equiv (dE_k/dk)/\hbar = 2t_0 a \sin(ka)/\hbar$, is maximal at $k_0 a = \pi/2$. It appears that on this scale, no reflectance occurs, in apparent agreement with Fig. 1 ($N = 2$, $m = 1$).

A closer look, however, indicates that some reflectance does indeed occur, as is illustrated in Fig. 3, which is a greatly expanded version of Fig. 2(b). Several characteristics are of note. First, the reflectance is non-zero. In fact, the amount of the wave packet reflected is indeed very tiny (see the scale!) and can readily be adjusted by changing the width α of the initial wave packet. These results are shown for $\alpha = 50a$, but a larger choice of the width α would reduce the reflectance accordingly. Essentially, the spread in wave vector about $k_0 a = 2\pi/3$ is inversely proportional to α . The larger α is, the more the wave packet approaches a mono-energetic wave packet with *only* $k_0 a = 2\pi/3$ and therefore perfect unit transmission (see Fig. 4 in Ref. 6).

Secondly, the reflected component is no longer Gaussian; in fact it appears to be a split wave packet with the peaks travelling coherently. Thirdly, distorted as these split wave packets are from the original in Fig. 2(b), they nonetheless retain their shape as a function of time. Note that because $k_0 a = 2\pi/3$, the wave packets do spread slightly with time, though it is difficult to see on this figure. For $k_0 a = \pi/2$ they do not spread at all, and the split Gaussian remains as it is for all the times shown. It is this remarkable line-shape that we want to more fully understand. As we will show in the next section, this split wave function can be described analytically by a single function that travels with wave vector k_0 .

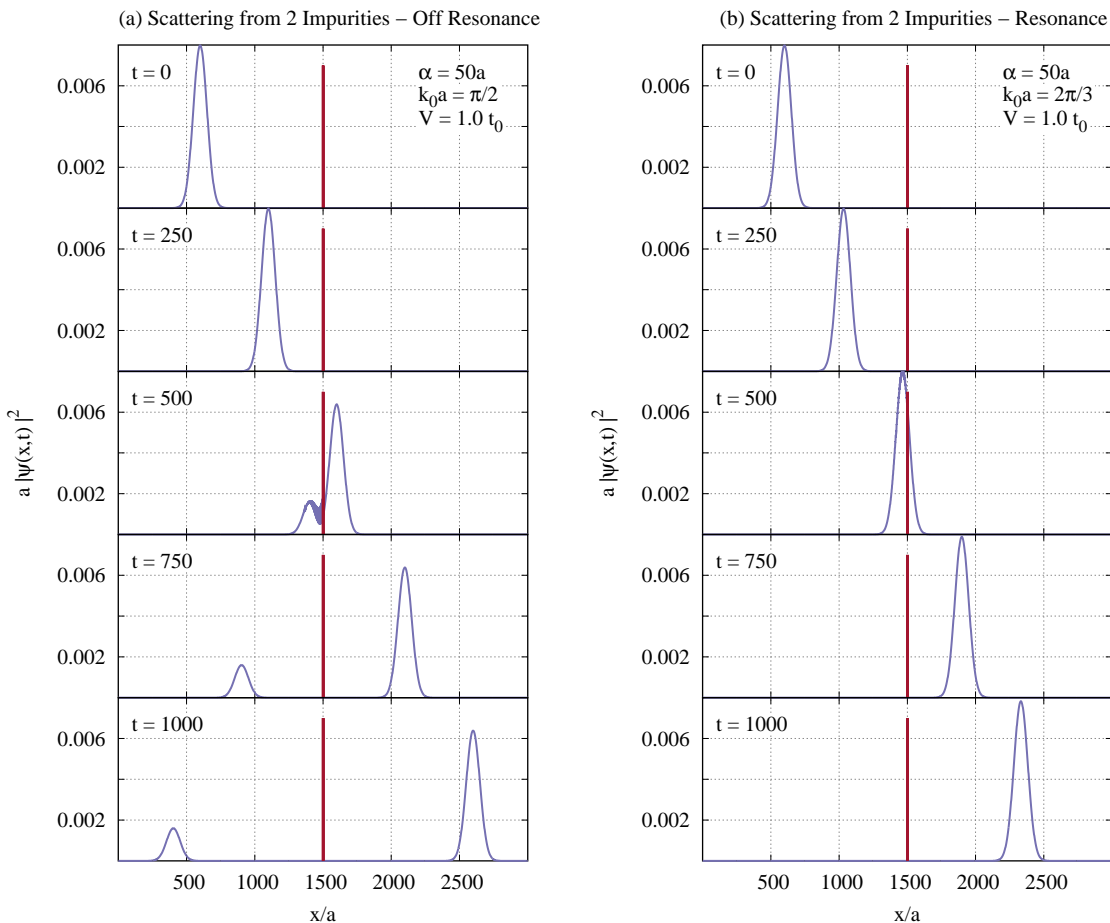


FIG. 2. Plots of $a|\psi(x_\ell, t)|^2$ as a function of lattice site for five different times (in units of \hbar/t_0) for (a) off resonance and (b) on resonance. The barrier (vertical bars) consists of two impurities, each with strength $V = 1.0t_0$ located at sites 1500 and 1501. We have illustrated wave packets for times well before scattering (the first two) and well after scattering (the last two). The wave-packet is initially centered at $x_\ell = 600a$. In plot (a) $k_0a = \pi/2$ and no spreading occurs because of the choice of k_0 , but a significant amount of reflection does occur. Note that no spreading occurs after scattering, in both the transmitted and reflected wave packets. In plot (b) $k_0a = 2\pi/3$ and is chosen according to the resonance condition Eq. (10) so that no reflection should occur, as appears to be the case here. On the other hand, wave packet broadening occurs as a function of time, as is (just barely) evident in the decreasing amplitude as a function of time. The actual presence of a small reflected component is shown in Fig. 3 below. In both cases, the scattering is elastic and the reflected wave packet propagates to the left and right with the same initial wave vector magnitude, k_0 .

A. Analytical approach to describe reflected and transmitted wave packets

The analytical expression for a wave packet in Eq. (17) follows from an integration over all wave vectors centered around $k \approx k_0$. The spread of the wave packet in real space α assures that only a small domain of wave vectors ($\Delta k \propto 1/\alpha$) surrounding k_0 is required, so that the energy dispersion can also be expanded around k_0 .

A similar expansion applies to both transmitted and reflected components (see Eq. (12) in Ref. 3). The re-

flected component is

$$\psi_R(x_\ell, t) = \frac{1}{\sqrt{2\pi}} \int_{-\infty}^{+\infty} dk \phi_{-k_0}(k) \rho(k) e^{ikx} e^{-iE_k t/\hbar}, \quad (18)$$

where the limits of integration have been extended to $\pm\infty$, $\rho(k)$ is the reflectance amplitude, and

$$\phi_{-k_0}(k) = \left(\frac{2\alpha^2}{\pi}\right)^{1/4} \exp\left[-\alpha^2(k+k_0)^2\right]. \quad (19)$$

The reflectance amplitude can be determined from the plane wave theory established in the previous Section II. Since this is an elastic scattering event, the reflected wave packet travels with the same energy as before the scattering event but in the negative x direction. The amplitude

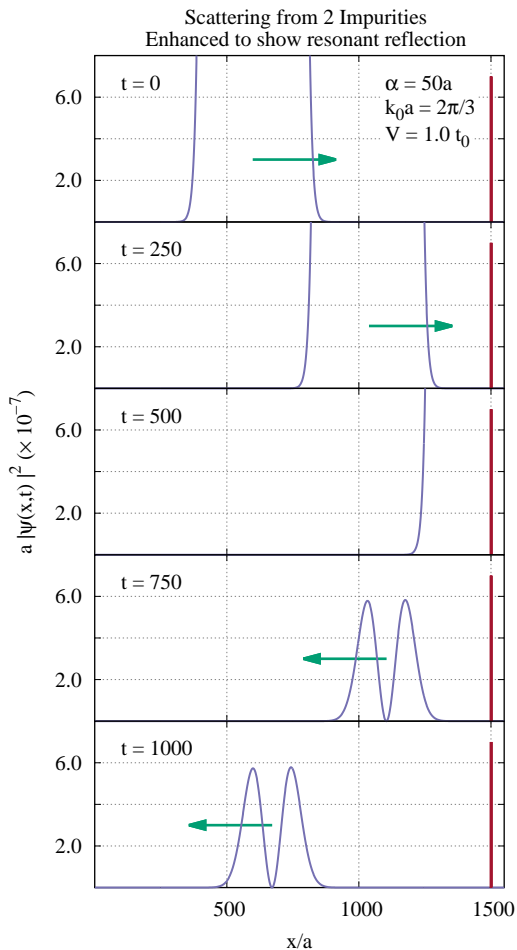


FIG. 3. An enlarged plot to show the reflected component of $a|\psi(x_\ell, t)|^2$ that is present in Fig. 2(b). See Fig. 2(b) for the initial wave packet and barrier parameters. Note the vertical scale here, consistent with the fact that the reflected profile in the two lowest panels were **not** visible in Fig. 2(b). Note also that the reflected wave packet profile ($t = 750\hbar/t_0$ and $1000\hbar/t_0$) *does not* consist of a single Gaussian wave packet; rather, *two* peaks are present for each time, and the expected centroid of the reflecting wave packet is precisely at the node between the two peaks. The reflected wave packet profile, though non-Gaussian, remains constant as a function of time, as seen visually by comparing the profile for the two times shown in the lowest two panels.

$\phi_{-k_0}(k)$ is hence indicated to have been evaluated for $-k_0$, as will be the reflectance amplitude $\rho(k)$ and the energy dispersion E_k .

By expanding $E(k)$ and $\rho(k)$ in Eq. (18) around $-k_0$, using the first order correction of $\rho(k)$, and the Gaussian form of $\phi(k)$, we can explicitly calculate the reflected probability $|\psi_R(x_\ell, t)|^2$ to first order. This approxima-

tion of Eq. (18) yields

$$\begin{aligned} \psi_R(x_\ell, t) &\approx \frac{\rho'(-k_0)}{\sqrt{2\pi}} \left(\frac{2\alpha^2}{\pi}\right)^{1/4} e^{-iE_0 t/\hbar} e^{-ixk_0} \\ &\times \int_{-\infty}^{+\infty} dk (k+k_0) e^{-[\alpha^2 + iE_0'' t/2\hbar](k+k_0)^2} e^{i(x-E_0' t/\hbar)(k+k_0)}. \end{aligned} \quad (20)$$

The above integral is Gaussian and can be done analytically. The probability is given by

$$|\psi_R(x_\ell, t)|^2 \approx \frac{|\rho'(k_0)|^2}{\sqrt{2\pi}} \frac{y^2(t) e^{-y^2(t)}}{2\alpha^2 \sqrt{\alpha^2 [1 + u^2(t)]}}, \quad (21)$$

where

$$u(t) \equiv \frac{E_{k_0}'' t}{2\hbar\alpha^2}, \quad (22)$$

and

$$y(t) \equiv \frac{(x_\ell - E_{k_0}' t/\hbar)}{\sqrt{2\alpha^2 [1 + u^2(t)]}}. \quad (23)$$

Here, $E_{k_0}' \equiv dE_k/dk$ evaluated at $k = k_0$, and similarly for E_{k_0}'' .

Equation (21) describes a “split” Gaussian function. The Gaussian is split because of the factor of $y^2(t)$ that precedes the exponential. The lower two panels in Fig. 3 make clear what a split Gaussian looks like. Note that for $k_0 a = \pm\pi/2$, $u(t) = 0$ since $E_{k_0}'' = 0$, so this expression describes a travelling split Gaussian whose width remains constant as a function of time for these particular wave vectors.

To understand how well Eq. (21) works we examine the reflection probability $R(k)$, which is determined from the reflectance amplitude as $R(k) = |\rho(k)|^2$. The reflectance amplitude is given by $\rho(k) = M_{12}/M_{22}$ as defined in the online Supplementary Material A. For the specific case $N = 2$ and $m = 1$, we can use the derived elements of the transfer matrix in Eq. (C3) to get

$$\rho(k) = ie^{2ika} \frac{f(k)}{1 - if(k)} \quad (24)$$

from which Eq. (9) immediately follows. The specific form of $f(k)$ for $N = 2$ and $m = 1$ is given below. Since we choose k_0 so that $\rho(k_0) = 0$, Eq. (20) came from the first order expansion, $\rho(k_0) \approx \rho'(k_0)(k - k_0)$, and therefore

$$R(k) \approx |\rho'(k_0)|^2 (k - k_0)^2. \quad (25)$$

This result is shown for $k_0 a = 2\pi/3$ in Fig. (4) (dashed red curve) since this is the wave vector for resonance to occur with $V = t_0$. This approximate expression for the reflection probability clearly compares favorably with the full reflection probability $R(k)$ computed from Eq. (9)

(solid green curve) only for a limited range of wave vectors close to k_0 .

Going to higher order in $k - k_0$ is possible and straightforward. For example, using that $f(k) \equiv v_k U_{N-1}(h_k)$, for the case $N = 2$ and $m = 1$ we find

$$f(k) = \frac{V(\cos(ka) + V/2t_0)}{t_0 \sin(ka)}. \quad (26)$$

By expanding both $\cos(ka)$ and $\sin(ka)$ around k_0 in the above expression, and by using the resonant condition Eq. (10) that gives us $\cos(k_0 a) + V/2t_0 = 0$, we obtain

$$\begin{aligned} f(k) &\approx \frac{V/t_0}{\sin(k_0 a) + a(k - k_0) \cos(k_0 a)} \\ &\times \left[\cos(k_0 a) - a(k - k_0) \sin(k_0 a) \right. \\ &\quad \left. - \frac{1}{2} a^2 (k - k_0)^2 \cos(k_0 a) + \frac{V}{2t_0} \right] \\ &\approx -\frac{V}{t_0} a (k - k_0) \left[1 - \frac{1}{2} a (k - k_0) \frac{\cos(k_0 a)}{\sin(k_0 a)} \right] \end{aligned} \quad (27)$$

where the correction in the next order of $a(k - k_0)$ is now included. Substituting Eq. (27) into Eq. (9), expanding about k_0 and evaluating the coefficients at $k_0 a = 2\pi/3$ and $V = t_0$ results in

$$R(k) \approx a^2 (k - k_0)^2 \left[1 + \frac{1}{\sqrt{3}} a (k - k_0) \right], \quad (28)$$

which is also shown in Fig. 4 as the dot-dashed blue curve. This result agrees with the full plane-wave result from Eq. (6) over a more extended range of k values around k_0 compared to the first order result. This correction may be useful as the wave packet width decreases, requiring more and more accuracy in the reflection coefficient for wave vectors further away from k_0 . Nonetheless, in the comparisons that follow we will use Eq. (25), which corresponds to just the first term in Eq. (28).

B. More detailed comparisons

In general, as the barrier width increases (i.e. as both N and m increase), we expect that the accuracy of this approximation will deteriorate (see Fig. 1). We wish to assess the analytic expression for the reflection probability given by Eq. (21), for a variety of barriers. For this purpose, we show in Fig. 5 the reflection probability as a function of position at some time (here, $t = 1000\hbar/t_0$) *well after* the incoming wave packet has scattered off the barrier. Note the vertical scale; we are zooming in on a very tiny amount of reflected wave packet. As in Fig. 3 we are using resonant scattering conditions in all cases, (i) $N = 3, m = 1$, (ii) $N = 3, m = 9$, (iii) $N = 6, m = 1$, and (iv) $N = 6, m = 9$, but here $k_0 a = \pi/2$ and $V = 1.0t_0$ for all barriers. The solid blue curve denotes the numerical calculation, while the dashed red curve denotes the analytical approximation given by Eq. (21). As is evident, when the width of the wave packet α greatly exceeds the

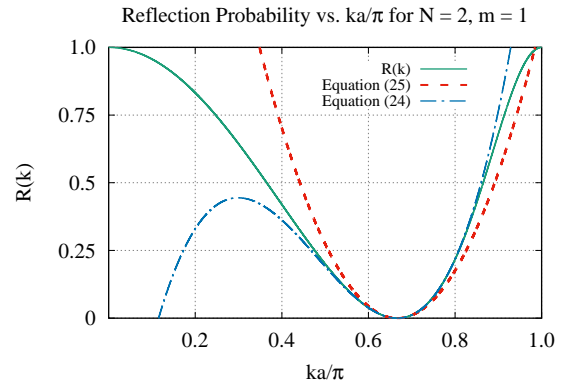


FIG. 4. Plot of the reflection probability $R(k)$ vs. ka/π (solid green curve). Also shown for comparison is the first order correction (Eq. (25), dotted red curve) along with the next order correction (Eq. (28), dot-dashed blue curve). The range of agreement is clearly extended by the next order correction. The parameters here are $k_0 a = 2\pi/3$, $V = t_0$, $N = 2$, and $m = 1$.

width of the barrier region w_B (cases (i) and (iii)), the approximation is excellent. As the barrier region width increases (cases (ii) and (iv)), the approximation begins to fail. Note that we are using $k_0 a = \pi/2$, so there is no deterioration of the Gaussian (or split Gaussian in the case of the reflected amplitude) as a function of time, and an identical result would hold for a later time as well. The accuracy of the analytical approximation in the two cases where the extension of the barrier is not so large (first and third panels) is remarkable given that the accuracy of the reflection probability used is similar to that shown in Fig. 4, and clearly works on a rather limited range about k_0 .

More general conditions for resonance can be readily determined. For example, for $V = t_0$, there is a resonant transmission that occurs at $k_0 a = \pi/2$ in all cases in which m is odd. A straightforward expansion of $f(k)$ [defined following Eq. (9)] for m odd, $V = t_0$ and $k_0 a = \pi/2$ results in

$$f(k) \approx -2ma(k - k_0), \quad \text{for } N = 3 \quad (29)$$

$$f(k) \approx -4ma(k - k_0), \quad \text{for } N = 6 \quad (30)$$

and similar formulas can be derived for other cases.

As expected, the agreement indeed deteriorates both as N increases and as m increases, as is apparent in Fig. 5(a). At the same time, we should remind the reader that we are capturing a tiny reflected component, so in some sense the second and fourth panels still show excellent qualitative agreement. For example, the fact that the original simple Gaussian wave packet shape has now been divided into a split Gaussian is captured magnificently by the approximate result shown here, based on Eq. (21).

To illustrate how improved agreement can be obtained systematically with increasing wave packet width, we show in Fig. 5(b) the results from Fig. 5(a), but now

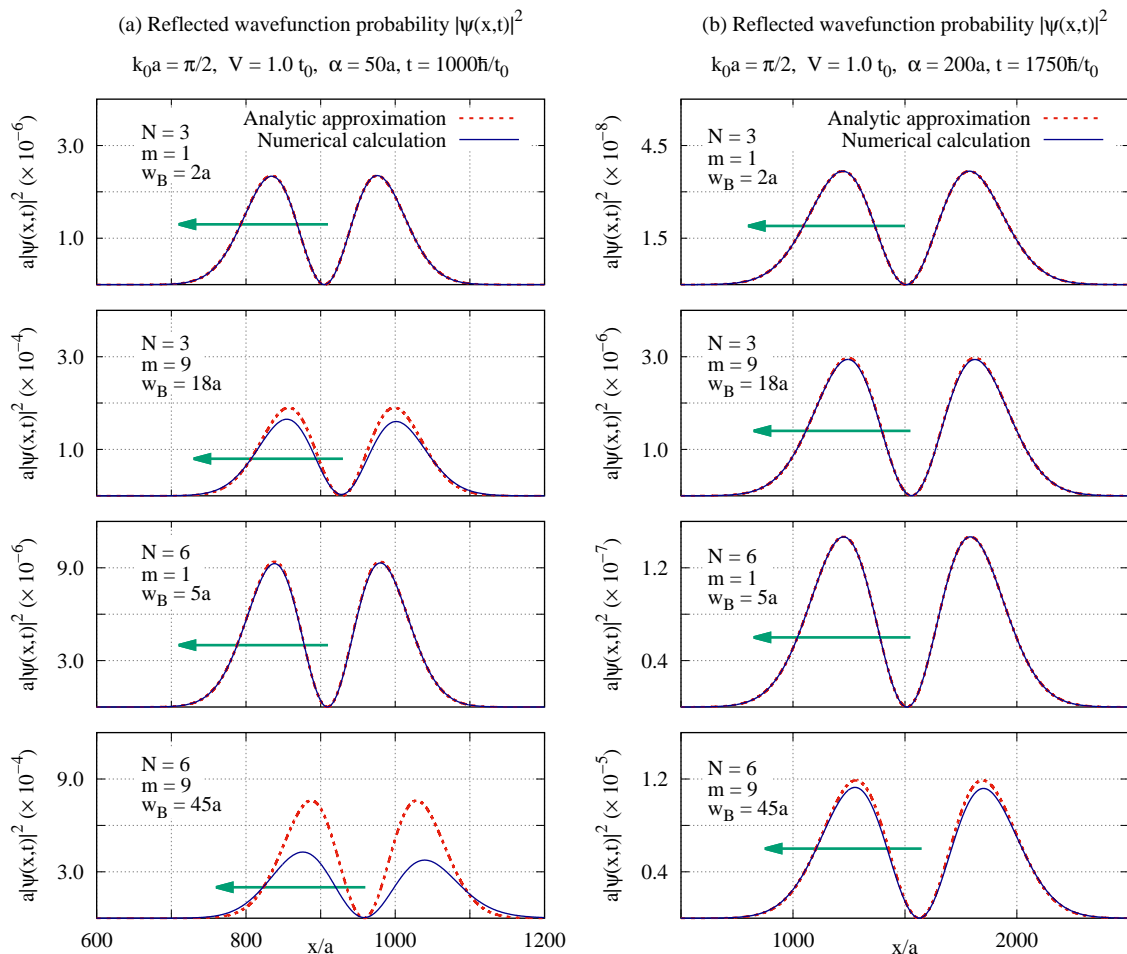


FIG. 5. The reflected component of $a|\psi(x_\ell, t)|^2$, after scattering has taken place at the barrier, as a function of lattice site for $t = 1000\hbar/t_0$ and the various barrier configurations as shown. The barrier starts at $x = 1500a$ (off-scale to the right). The results are determined both numerically (solid blue curves) and analytically through Eq. (21) (dashed red curves). The wave packet has $k_0a = \pi/2$, and starts at $t = 0$ from $x_0 = 600a$, with (a) $\alpha = 50a$ and (b) $\alpha = 200a$. In all these cases the transmission resonance condition is satisfied (see Eq. (30)). Note the vertical scale in this figure, consistent with the expectation that these components are nominal. All are in qualitative agreement and quantitatively improve as the wave packet width is increased with respect to the barrier length.

for the wider wave packet with $\alpha = 200a$. There is clear quantitative improvement for all panels, most evident in the second and fourth panels. Clearly one of the issues with the poorer agreement in Fig. 5(a) is that the barrier width is comparable to the width of the wave packet. For example in the fourth panel the barrier width w_B is $45a$, which is very close to the width of the wave packet $\alpha = 50a$ that is used. With a wave packet width of $\alpha = 200a$, we arrive at a situation where the wave packet width is much greater than any length scale associated with the barrier, and of course, for still larger values of α the agreement with the numerical results improves still further.

Conversely, for smaller values of α , the agreement deteriorates considerably. In Fig. 6 we show the same four cases as in Fig. 5(a) and (b), but now with $\alpha = 5a$. Even for just three barriers (located at sites 1500, 1501, and

1502), there is no remnant of a split Gaussian, and in fact there is even a deterioration of the lineshape as a function of time, indicating that the expansion behind the analytical derivation of Eq. (17) has lost its validity. The approximate result provided by Eq. (21) is shown in the first panel only (dashed red curve), and is qualitatively incorrect. The results for such a narrow wave packet cannot be described with the help of the plane wave theory, as scattering events at the individual components of the barriers are disconnected, and can no longer interfere with one another.

IV. SUMMARY

We have formulated the one-dimensional scattering problem on a lattice to study the effect of a non-infinite

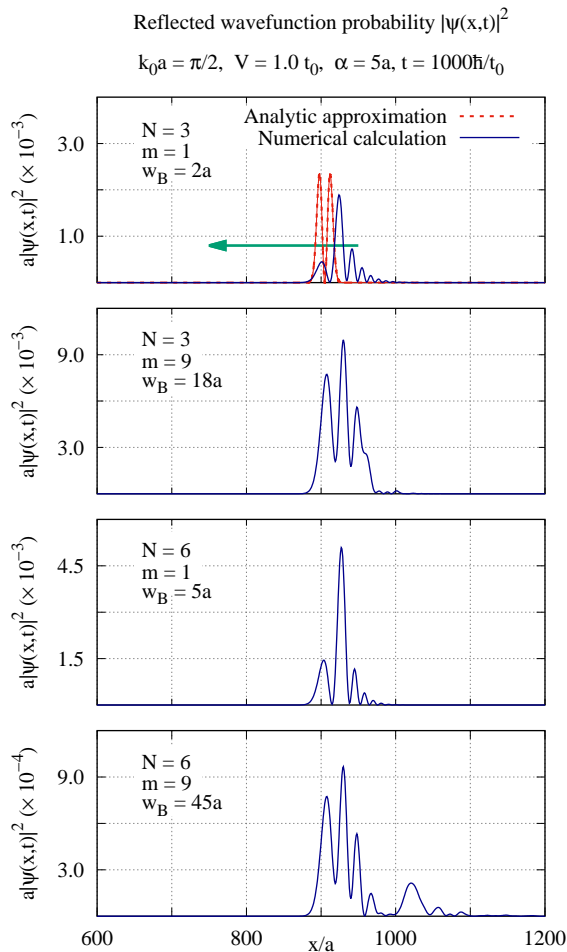


FIG. 6. As Fig. 5 but now for a narrower wave packet with $\alpha = 5a$. As before we show only the reflected components of $a|\psi(x_\ell, t)|^2$ as a function of lattice site for $t = 1000\hbar/t_0$ and the various barrier configurations as shown. The barrier starts at $x = 1500a$ (off-scale to the right). The results are determined both numerically (solid blue curves) and analytically through Eq. (21) (dashed red curve in the first panel). The reflected portion is still small, though the vertical scale is now several orders of magnitude higher than in Fig. 5. The numerical results have significantly distorted shapes, and can no longer be described by split Gaussian wave packets.

wave packet width on the transmission and reflection coefficients. As much as possible, we have focussed on the wave vector $k_0 a = \pi/2$ so that the Gaussian wave packet that we use retains the same width for extended periods of time. We emphasize that having a constant width as a function of time is an approximate result based on a Taylor expansion in the exponential, but the numerical results presented in this paper do not use this approximation, and nevertheless demonstrate this characteristic for the time scales involved in the scattering process. This makes the use of these wave packets a helpful tool, since all changes can be attributed to the scattering process, and *not* to the general time evolution of the wave packet itself. Moreover, conceptually, it is easier to think of

these wave packets as actual particles used in the beam experiment — they actually move towards and scatter off and move away from the target as a function of time. This is in contrast to the plane wave description, where time has disappeared from the problem, and incoming, scattering and outgoing particles appear to the novice to be present at all times and in all places in a sort of steady-state condition.

We also focussed on barrier potentials that result in resonant transmission for a mono-energetic plane wave, namely $V = t_0$ for the four cases considered in the last three figures. Then any reflection can be attributed to the fact that a finite width wave packet was used in the scattering process. We found numerically that a minute amount was reflected, but the reflected component had a well defined and peculiar split Gaussian profile. Based on these results we devised an approximation for the reflected component, Eq. (21) which, when combined with a simple approximation for the reflectivity as a function of wave vector, yields excellent results compared to the exact numerical results. For reasonably large wave packet widths, we find quantitative agreement for the reflected wave profile, and a good understanding of its accuracy based on the initial Gaussian width. In this way a combination of plane wave-based reflection coefficients (Fig. 1), together with analytical wave packet dynamics allows us a more insightful understanding of the time dependence of the scattering process off of simple barriers. At the same time, for wave packets whose width is less than the characteristic barrier length scale, the scattering description in terms of plane waves breaks down completely, as the results of Fig. 6 show.

ACKNOWLEDGMENTS

This work was supported in part by the Natural Sciences and Engineering Research Council of Canada (NSERC) and by an MIF from the Province of Alberta.

The authors have no conflicts to disclose.

Supplementary Material

Appendix A: Transfer Matrix

The solution to the one-dimensional quantum mechanical scattering problem in the presence of a localized potential $V(x)$ using the transfer matrix method has been investigated extensively.⁸⁻¹³ We review this work in this Appendix, both to keep this work self-contained, and to define various terms for the specific application of wave packet propagation in the tight binding model.

The transfer matrix relates the amplitudes of propagating waves between the left and right side of a barrier V . In the continuum, a general solution to the time-independent Schrödinger equation

$$-\frac{\hbar^2}{2m} \frac{d^2 \psi(x)}{dx^2} + V(x) \psi(x) = E \psi(x), \quad (\text{A1})$$

is required, where $V(x)$ is defined on the interval (a, b) . In general the wave function is given by

$$\psi(x) = \begin{cases} Ae^{ikx} + Be^{-ikx} & \text{for } x < a \\ \psi_{ab}(x) & \text{for } a < x < b \\ Ce^{ikx} + De^{-ikx} & \text{for } x > b. \end{cases} \quad (\text{A2})$$

The scattering matrix \mathbf{S} relates the incoming and outgoing wave function components as

$$\begin{pmatrix} B \\ C \end{pmatrix} = \mathbf{S} \begin{pmatrix} A \\ D \end{pmatrix} = \begin{pmatrix} S_{11} & S_{12} \\ S_{21} & S_{22} \end{pmatrix} \begin{pmatrix} A \\ D \end{pmatrix},$$

while the transfer matrix \mathbf{M} relates the wave function components between the left side and right side of the barrier as

$$\begin{pmatrix} C \\ D \end{pmatrix} = \mathbf{M} \begin{pmatrix} A \\ B \end{pmatrix} = \begin{pmatrix} M_{11} & M_{12} \\ M_{21} & M_{22} \end{pmatrix} \begin{pmatrix} A \\ B \end{pmatrix}.$$

These two descriptions above are related as⁹

$$\mathbf{M} = \begin{pmatrix} S_{21} - \frac{S_{22}S_{11}}{S_{12}} & \frac{S_{22}}{S_{12}} \\ -\frac{S_{11}}{S_{12}} & \frac{1}{S_{12}} \end{pmatrix}. \quad (\text{A3})$$

The elements of the scattering matrix \mathbf{S} give us the transmission amplitude from right to left of the barrier $\tau = S_{12}$ and left to right $\tau' = S_{21}$, and the reflection amplitudes on each side of the barrier $\rho = S_{22}$ and $\rho' = S_{11}$. We can write the scattering matrix as

$$\mathbf{S} = \begin{pmatrix} \rho' & \tau \\ \tau' & \rho \end{pmatrix}. \quad (\text{A4})$$

The transmission (reflection) coefficient is then defined as the probability that a particle is transmitted (reflected) by $T = |\tau|^2$ ($R = |\rho|^2$).

Furthermore, it can be shown⁹ that time reversal symmetry and conservation of current density further restrict

the elements of \mathbf{M} and \mathbf{S} . Following Ref. 9, time-reversal symmetry leads to the conclusion that the scattering matrix \mathbf{S} is unitary. This gives us the relation (one of four, see Eq. (1.26) in Ref. 9) that $S_{11}^* S_{12} + S_{12}^* S_{22} = (\rho')^* \tau + (\tau')^* \rho = 0$. This lets us write

$$\frac{\rho}{\tau} = - \left(\frac{\rho'}{\tau'} \right)^*, \quad (\text{A5})$$

and we can use this to simplify the element M_{11} in Eq. (A3) as

$$M_{11} = \tau' - \frac{\rho\rho'}{\tau} = \tau' + \left(\frac{\rho'}{\tau'} \right)^* \rho' = \frac{|\tau'|^2 + |\rho'|^2}{(\tau')^*}. \quad (\text{A6})$$

Conservation of current density leads to the relation that $|\tau'|^2 + |\rho'|^2 = |\tau|^2 + |\rho|^2 = 1$, which lets us simplify the transfer matrix to the following form

$$\mathbf{M} = \begin{pmatrix} \frac{1}{(\tau')^*} & \frac{\rho}{\tau} \\ -\frac{\rho'}{\tau} & \frac{1}{\tau} \end{pmatrix}. \quad (\text{A7})$$

Appendix B: Tight-Binding Model and Single Impurity

The tight-binding Hamiltonian for a 1D lattice with N impurities is

$$H = -t_0 \sum_{\ell} [c_{\ell}^{\dagger} c_{\ell+1} + c_{\ell+1}^{\dagger} c_{\ell}] + \sum_{\ell=1}^N V_{\ell} c_{\ell}^{\dagger} c_{\ell} \quad (\text{B1})$$

and the corresponding Schrödinger equation is

$$-t_0 [\psi_{\ell+1} + \psi_{\ell-1}] + V_{\ell} \psi_{\ell} = E_k \psi_{\ell}. \quad (\text{B2})$$

This Hamiltonian assumes nearest-neighbor hopping only. Equivalently, the Schrödinger equation (Eq. B2) can be written as the matrix equation

$$\begin{pmatrix} \psi_{\ell+1} \\ \psi_{\ell} \end{pmatrix} = \begin{pmatrix} \tilde{V}_{\ell} - \tilde{E}_k & -1 \\ 1 & 0 \end{pmatrix} \begin{pmatrix} \psi_{\ell} \\ \psi_{\ell-1} \end{pmatrix} \quad (\text{B3})$$

$$= \mathbf{P}_{\ell} \begin{pmatrix} \psi_{\ell} \\ \psi_{\ell-1} \end{pmatrix}. \quad (\text{B4})$$

where $\tilde{V} \equiv V/t_0$ and $\tilde{E} = E/t_0$. We assume that a wave function at a site ℓ (at coordinate x_{ℓ}) is of the form $\psi_{\ell} = Ae^{ikx_{\ell}} + Be^{-ikx_{\ell}}$.

Our aim is to find the transfer matrix that relates the amplitudes of a wave function that satisfies Eq.(B2) at lattice site x_{ℓ} with those at the nearest neighbour site $x_{\ell+1}$. So if $\psi_{\ell} = Ae^{ikx_{\ell}} + Be^{-ikx_{\ell}}$ and $\psi_{\ell+1} = Ce^{ikx_{\ell+1}} + De^{-ikx_{\ell+1}}$, we define a matrix \mathbf{M}_{ℓ} that satisfies

$$\begin{pmatrix} C e^{ikx_{\ell+1}} \\ D e^{-ikx_{\ell+1}} \end{pmatrix} = \mathbf{M}_{\ell} \begin{pmatrix} A e^{ikx_{\ell}} \\ B e^{-ikx_{\ell}} \end{pmatrix}, \quad (\text{B5})$$

We now write \mathbf{M}_n in terms of the Schrödinger equation Eq. (B2).

The wave function at lattice site ℓ , $\psi_\ell = Ae^{ikx_\ell} + Be^{-ikx_\ell} = Ae^{ik\ell a} + Be^{-ik\ell a}$, can be expressed as the matrix equation

$$\begin{pmatrix} \psi_\ell \\ \psi_{\ell-1} \end{pmatrix} = \begin{pmatrix} 1 & 1 \\ e^{-ika} & e^{ika} \end{pmatrix} \begin{pmatrix} Ae^{ik\ell a} \\ Be^{-ik\ell a} \end{pmatrix} \quad (\text{B6})$$

$$= \mathbf{Q} \begin{pmatrix} Ae^{ik\ell a} \\ Be^{-ik\ell a} \end{pmatrix}, \quad (\text{B7})$$

where \mathbf{Q} is just the matrix to give back the correct form of ψ_ℓ and $\psi_{\ell-1}$, and similarly for $\psi_{\ell+1}$,

$$\begin{pmatrix} \psi_{\ell+1} \\ \psi_\ell \end{pmatrix} = \begin{pmatrix} 1 & 1 \\ e^{-ika} & e^{ika} \end{pmatrix} \begin{pmatrix} Ce^{ik(\ell+1)a} \\ De^{-ik(\ell+1)a} \end{pmatrix} \quad (\text{B8})$$

$$= \mathbf{Q} \begin{pmatrix} Ce^{ik(\ell+1)a} \\ De^{-ik(\ell+1)a} \end{pmatrix}. \quad (\text{B9})$$

We can use the above expressions and Eq. (B3) to rewrite

Eq. (B5) as

$$\begin{pmatrix} Ce^{ik(\ell+1)a} \\ De^{-ik(\ell+1)a} \end{pmatrix} = \mathbf{Q}^{-1} \begin{pmatrix} \psi_{\ell+1} \\ \psi_\ell \end{pmatrix} \quad (\text{B10})$$

$$= \mathbf{Q}^{-1} \mathbf{P}_\ell \begin{pmatrix} \psi_\ell \\ \psi_{\ell-1} \end{pmatrix} \quad (\text{B11})$$

$$= \mathbf{Q}^{-1} \mathbf{P}_\ell \mathbf{Q} \begin{pmatrix} Ae^{ik\ell a} \\ Be^{-ik\ell a} \end{pmatrix} \quad (\text{B12})$$

$$= \mathbf{M}_\ell \begin{pmatrix} Ae^{ik\ell a} \\ Be^{-ik\ell a} \end{pmatrix} \quad (\text{B13})$$

where the transfer matrix is given by $\mathbf{M}_\ell = \mathbf{Q}^{-1} \mathbf{P}_\ell \mathbf{Q}$.

Using the explicit forms of \mathbf{P}_ℓ and \mathbf{Q} we calculate \mathbf{M}_ℓ explicitly

$$\mathbf{M}_\ell = \mathbf{Q}^{-1} \mathbf{P}_\ell \mathbf{Q} \quad (\text{B14})$$

$$\begin{aligned} &= \frac{1}{2i \sin(ka)} \begin{pmatrix} e^{ika} & -1 \\ -e^{-ika} & 1 \end{pmatrix} \begin{pmatrix} \tilde{V}_\ell - \tilde{E}_k & -1 \\ 1 & 0 \end{pmatrix} \begin{pmatrix} 1 & 1 \\ e^{-ika} & e^{ika} \end{pmatrix} \\ &= \frac{1}{2i \sin(ka)} \begin{pmatrix} -2 + e^{ika} (\tilde{V}_\ell - \tilde{E}_k) & -1 - e^{2ika} + e^{ika} (\tilde{V}_\ell - \tilde{E}_k) \\ 1 + e^{2ika} - e^{-ika} (\tilde{V}_\ell - \tilde{E}_k) & 2 - e^{-ika} (\tilde{V}_\ell - \tilde{E}_k) \end{pmatrix} \end{aligned} \quad (\text{B15})$$

In the tight-binding model, the dispersion relation is given by $E_k = -2t_0 \cos(ka)$. Substituting this into the above equation (with $t_0 = 1$) and simplifying gives us the transfer matrix for lattice site ℓ ,

$$\begin{aligned} \mathbf{M}_\ell &= \begin{pmatrix} e^{ika} \left[1 + \frac{\tilde{V}_\ell}{2i \sin(ka)} \right] & e^{ika} \frac{\tilde{V}_\ell}{2i \sin(ka)} \\ -e^{-ika} \frac{\tilde{V}_\ell}{2i \sin(ka)} & e^{-ika} \left[1 - \frac{\tilde{V}_\ell}{2i \sin(ka)} \right] \end{pmatrix}. \end{aligned} \quad (\text{B16})$$

The probability for transmission for a single impurity is then easily calculated from the above expression as

$$\begin{aligned} T &= \frac{1}{|M_{22}|^2} = \frac{1}{1 + \tilde{V}_\ell^2 \frac{1}{4 \sin^2(ka)}} \\ &= \frac{\sin^2(ka)}{\sin^2(ka) + V_\ell^2 / 4t_0^2}. \end{aligned} \quad (\text{B17})$$

For the case where there are no impurities the transfer matrix Eq. (B16) simplifies to

$$\mathbf{M}^{(1)} = \begin{pmatrix} e^{ika} & 0 \\ 0 & e^{-ika} \end{pmatrix} \quad (\text{B18})$$

and gives a simple one lattice ‘‘hop’’ satisfying Eq. (B5). For m impurity free hops this simply extends to multiplying $\mathbf{M}^{(1)}$ m times, which gives

$$\mathbf{M}^{(m)} = \begin{pmatrix} e^{ika} & 0 \\ 0 & e^{-ika} \end{pmatrix}^m = \begin{pmatrix} e^{ikma} & 0 \\ 0 & e^{-ikma} \end{pmatrix}. \quad (\text{B19})$$

Appendix C: Dimers and Generalization to N Impurities

With the general transfer matrix for a single site ℓ , we can calculate the transfer matrix (and therefore the transmission and reflection amplitudes) of a system of two impurities separated by m lattice sites. This configuration is referred to as a dimer and has been explored extensively in Refs. 2, 3, 16–20.

Let V_ℓ be the potential at a site ℓ , and $V_{\ell+m}$ the potential at a site m lattice spacings away at $\ell+m$. We will assume that these two potentials are of equal strength $V_\ell = V_{\ell+m} = V$. Between these two potentials there are $m-1$ sites where $V_i = 0$.

For such a configuration the wave function amplitude on the left-hand-side of the entire barrier (dimer) can be seen as encountering the first impurity V_ℓ , described by a transfer matrix \mathbf{M}_1 , freely propagating over $m-1$ lattice sites, described by $\mathbf{M}^{(m-1)}$, and finally encountering the second impurity $V_{\ell+m}$, described by \mathbf{M}_2 . The transfer matrix describing the dimer is given by $\mathbf{M} = \mathbf{M}_1 \mathbf{M}^{(m-1)} \mathbf{M}_2$.

Since $V_\ell = V_{\ell+m} = V$, we have $\mathbf{M}_1 = \mathbf{M}_2$ given by

Eq. (B16) ($\tilde{V} = V/t_0$)

$$\begin{aligned} \mathbf{M}_1 &= \mathbf{M}_2 \\ &= \begin{pmatrix} e^{ika} \left(1 + \frac{\tilde{V}}{2i \sin(ka)}\right) & e^{ika} \frac{\tilde{V}}{2i \sin(ka)} \\ -e^{-ika} \frac{\tilde{V}}{2i \sin(ka)} & e^{-ika} \left(1 - \frac{\tilde{V}}{2i \sin(ka)}\right) \end{pmatrix}. \end{aligned} \quad (\text{C1})$$

Calculating the transfer matrix explicitly for the system gives

$$\begin{aligned} \mathbf{M} &= \mathbf{M}_1 \mathbf{M}^{(m-1)} \mathbf{M}_2 \\ &= \begin{pmatrix} e^{ika} \left(1 + \frac{\tilde{V}}{2i \sin(ka)}\right) & e^{ika} \frac{\tilde{V}}{2i \sin(ka)} \\ -e^{-ika} \frac{\tilde{V}}{2i \sin(ka)} & e^{-ika} \left(1 - \frac{\tilde{V}}{2i \sin(ka)}\right) \end{pmatrix} \begin{pmatrix} e^{ika(m-1)} & 0 \\ 0 & e^{-ika(m-1)} \end{pmatrix} \begin{pmatrix} e^{ika} \left(1 + \frac{\tilde{V}}{2i \sin(ka)}\right) & e^{ika} \frac{\tilde{V}}{2i \sin(ka)} \\ -e^{-ika} \frac{\tilde{V}}{2i \sin(ka)} & e^{-ika} \left(1 - \frac{\tilde{V}}{2i \sin(ka)}\right) \end{pmatrix} \end{aligned} \quad (\text{C2})$$

with the elements of \mathbf{M} simplifying to

$$\begin{aligned} M_{11} &= e^{ika(m+1)} \left(1 + \frac{\tilde{V}}{2i \sin(ka)}\right)^2 - e^{-ika(m-1)} \left(\frac{\tilde{V}}{2i \sin(ka)}\right)^2 \\ M_{22} &= e^{-ika(m+1)} \left(1 - \frac{\tilde{V}}{2i \sin(ka)}\right)^2 - e^{ika(m-1)} \left(\frac{\tilde{V}}{2i \sin(ka)}\right)^2 = M_{(1,1)}^* \\ M_{12} &= \frac{\tilde{V}}{2i \sin(ka)} \left[e^{ika(m+1)} \left(1 + \frac{\tilde{V}}{2i \sin(ka)}\right) + e^{-ika(m-1)} \left(1 - \frac{\tilde{V}}{2i \sin(ka)}\right) \right] \\ M_{21} &= \frac{-\tilde{V}}{2i \sin(ka)} \left[e^{-ika(m+1)} \left(1 - \frac{\tilde{V}}{2i \sin(ka)}\right) + e^{ika(m-1)} \left(1 + \frac{\tilde{V}}{2i \sin(ka)}\right) \right] = M_{(1,2)}^*. \end{aligned} \quad (\text{C3})$$

From this transfer matrix we calculate

$$\begin{aligned} |M_{22}|^2 &= M_{11} \times M_{22} \\ &= \left[e^{ika(m+1)} \left(1 + \frac{\tilde{V}}{2i \sin(ka)}\right)^2 - e^{-ika(m-1)} \left(\frac{\tilde{V}}{2i \sin(ka)}\right)^2 \right] \\ &\quad \times \left[e^{-ika(m+1)} \left(1 - \frac{\tilde{V}}{2i \sin(ka)}\right)^2 - e^{ika(m-1)} \left(\frac{\tilde{V}}{2i \sin(ka)}\right)^2 \right] \\ &= \frac{1}{\sin^2(ka)} \left[\sin^2(ka) + \tilde{V}^2 \left(\cos(kam) + \frac{\tilde{V} \sin(kam)}{2 \sin(ka)} \right)^2 \right], \end{aligned} \quad (\text{C4})$$

which gives the transmission probability for a dimer of length m as²

$$T = \frac{\sin^2(ka)}{\sin^2(ka) + \tilde{V}^2 \left[\cos(kam) + \frac{\tilde{V} \sin(kam)}{2 \sin(ka)} \right]^2}. \quad (\text{C5})$$

We now extend this calculation to a series of N equal-strength impurities, each separated by $m-1$ lattice sites.

For simplicity we define the parameters

$$g = e^{ika} \quad (\text{C6})$$

$$v_k = \frac{\tilde{V}}{2 \sin(ka)} \quad (\text{C7})$$

so that the transfer matrix for a single impurity has the

form

$$\mathbf{M}_1 = \begin{pmatrix} g(1-iv_k) & -igv_k \\ ig^*v_k & g^*(1+iv_k) \end{pmatrix}, \quad (\text{C8})$$

and

$$\mathbf{M}^{(m)} = \begin{pmatrix} g^m & 0 \\ 0 & g^{*m} \end{pmatrix}. \quad (\text{C9})$$

For N impurities, the transfer matrix for the system is $\mathbf{M} = \mathbf{M}_1 \mathbf{M}^{(m-1)} \mathbf{M}_2 \cdots \mathbf{M}^{(m-1)} \mathbf{M}_N$, where $\mathbf{M}_1 = \mathbf{M}_2 = \cdots = \mathbf{M}_N$ for equal-strength impurities. We therefore need to calculate the matrix product $\mathbf{M} = \mathbf{M}_1 \left(\mathbf{M}^{(m-1)} \mathbf{M}_1 \right)^{(N-1)}$. For a unimodular matrix \mathbf{A} , $\det \mathbf{A} = 1$, the Chebyshev identity²¹ gives us

$$\begin{aligned} \mathbf{A}^N &= \begin{pmatrix} A_{11} & A_{12} \\ A_{21} & A_{22} \end{pmatrix}^N \\ &= \begin{pmatrix} A_{11}U_{N-1}(h) - U_{N-2}(h) & A_{12}U_{N-1}(h) \\ A_{21}U_{N-1}(h) & A_{22}U_{N-1}(h) - U_{N-2}(h) \end{pmatrix} \end{aligned}$$

where

$$h = \frac{1}{2}(A_{11} + A_{22}) \quad (\text{C10})$$

and U_N is the Chebyshev polynomial of the second kind. For $\mathbf{M}^{(m-1)} \mathbf{M}_1$,

$$\begin{aligned} \mathbf{M}^{(m-1)} \mathbf{M}_1 &= \begin{pmatrix} g^{(m-1)} & 0 \\ 0 & g^{*(m-1)} \end{pmatrix} \begin{pmatrix} g(1-iv_k) & -igv_k \\ ig^*v_k & g^*(1+iv_k) \end{pmatrix} \\ &= \begin{pmatrix} g^m(1-iv_k) & -ig^m v_k \\ ig^{*m} v_k & g^{*m}(1+iv_k) \end{pmatrix} \end{aligned} \quad (\text{C11})$$

and

$$\begin{aligned} h_k &= \frac{1}{2}(M_{11} + M_{22}) \\ &= \frac{1}{2}(g^m(1-iv_k) + g^{*m}(1+iv_k)) \\ &= \frac{1}{2}(g^m + g^{*m} - iv_k(g^m - g^{*m})) \\ &= \frac{1}{2}(e^{ikam} + e^{-ikam} - iv_k(e^{ikam} - e^{-ikam})) \\ &= \cos(kam) + v_k \sin(kam). \end{aligned} \quad (\text{C12})$$

Calculating the $(N-1)^{th}$ power gives us

$$\left(\mathbf{M}^{(m-1)} \mathbf{M}_1 \right)^{N-1} = \begin{pmatrix} g^m(1-iv_k)U_{N-2}(h_k) - U_{N-3}(h_k) & -ig^m v_k U_{N-2}(h_k) \\ ig^{*m} v_k U_{N-2}(h_k) & g^{*m}(1+iv_k)U_{N-2}(h_k) - U_{N-3}(h_k) \end{pmatrix} \quad (\text{C13})$$

The transfer matrix \mathbf{M} for N potentials, each separated by m lattice sites is

$$\begin{aligned} \mathbf{M} &= \mathbf{M}_1 \left(\mathbf{M}^{(m-1)} \mathbf{M}_1 \right)^{N-1} \\ &= \begin{pmatrix} g(1-iv_k) & -igv_k \\ ig^*v_k & g^*(1+iv_k) \end{pmatrix} \begin{pmatrix} g^m(1-iv_k)U_{N-2}(h_k) - U_{N-3}(h_k) & -ig^m v_k U_{N-2}(h_k) \\ ig^{*m} v_k U_{N-2}(h_k) & g^{*m}(1+iv_k)U_{N-2}(h_k) - U_{N-3}(h_k) \end{pmatrix}. \end{aligned} \quad (\text{C14})$$

For the transmission probability we only need to calculate M_{11} from the above expression since $T = 1/|M_{22}|^2 = 1/|M_{11}|^2$. Following from Eq. (C14)

$$\begin{aligned} M_{11} &= g(1-iv_k)g^m(1-iv_k)U_{N-2}(h_k) - g(1-iv_k)U_{N-3}(h_k) - igv_k ig^{*m} v_k U_{N-2}(h_k) \\ &= \left[g^{m+1}(1-iv_k)^2 + g^{*(m-1)} v_k^2 \right] U_{N-2}(h_k) - g(1-iv_k)U_{N-3}(h_k) \end{aligned} \quad (\text{C15})$$

and

$$\begin{aligned} |M_{11}|^2 &= \left(\left[g^{m+1}(1-iv_k)^2 + g^{*(m-1)} v_k^2 \right] U_{N-2}(h_k) - g(1-iv_k)U_{N-3}(h_k) \right) \\ &\quad \times \left(\left[g^{*(m+1)}(1+iv_k)^2 + g^{(m-1)} v_k^2 \right] U_{N-2}(h_k) - g^*(1+iv_k)U_{N-3}(h_k) \right) \\ &= \left[g^{m+1}(1-iv_k)^2 + g^{*(m-1)} v_k^2 \right] \left[g^{*(m+1)}(1+iv_k)^2 + g^{(m-1)} v_k^2 \right] U_{N-2}^2(h_k) \\ &\quad - g^*(1+iv_k) \left[g^{m+1}(1-iv_k)^2 + g^{*(m-1)} v_k^2 \right] U_{N-2}(h_k) U_{N-3}(h_k) \\ &\quad - g(1-iv_k) \left[g^{*(m+1)}(1+iv_k)^2 + g^{(m-1)} v_k^2 \right] U_{N-2}(h_k) U_{N-3}(h_k) \\ &\quad + g(1-iv_k)g^*(1+iv_k)U_{N-3}^2(h_k) \end{aligned} \quad (\text{C16})$$

Simplifying all these terms yields

$$|M_{11}|^2 = U_{N-2}^2(h_k)(1 + 4h_k^2 v_k^2) - U_{N-2}(h_k)U_{N-3}(h_k)2h_k(1 + 2v_k^2) + U_{N-3}^2(h_k)(1 + v_k^2) \quad (\text{C17})$$

One can further simplify this equation above by using the recursion relations for U_N ,

$$U_{N+1}(x) = 2xU_N(x) - U_{N-1}(x), \quad (\text{C18})$$

and the expression that (proof in the following section)

$$U_{N-2}^2(x) - 2xU_{N-2}(x)U_{N-3}(x) + U_{N-3}^2(x) = 1, \quad (\text{C19})$$

one then obtains

$$\begin{aligned} |M_{11}|^2 &= U_{N-2}^2(h_k)(1 + 4h_k^2 v_k^2) - U_{N-2}(h_k)U_{N-3}(h_k)2h_k(1 + 2v_k^2) + U_{N-3}^2(h_k)(1 + v_k^2) \\ &= 1 + v_k^2 U_{N-1}^2(h_k). \end{aligned} \quad (\text{C20})$$

The general expression for the transmission through N potentials, each separated by m lattice sites is therefore^{9,13}

$$T = \frac{1}{1 + v_k^2 U_{N-1}^2(h)}, \quad (\text{C21})$$

where $U_N(h)$ is the N^{th} Chebyshev polynomial, and

$$h = \cos(kam) + v_k \sin(kam) \quad (\text{C22})$$

$$v_k = \frac{V}{2t_0 \sin(ka)}. \quad (\text{C23})$$

Appendix D: Proof of $U_{N-2}^2 - 2hU_{N-2}U_{N-3} + U_{N-3}^2 = 1$ for all N

The recursion relation for Chebyshev polynomials of the second kind is

$$\begin{aligned} U_0(h) &= 1 \\ U_1(h) &= 2h \\ U_2(h) &= 4h^2 - 1 \\ U_3(h) &= 8h^3 - 4h \\ U_4(h) &= 16h^4 - 12h^2 + 1 \\ U_n(h) &= 2hU_{n-1}(h) - U_{n-2}(h). \end{aligned} \quad (\text{D1})$$

Let $k = N - 2$, we define

$$d(k) \equiv U_k^2 - 2hU_kU_{k-1} + U_{k-1}^2. \quad (\text{D2})$$

It is easy to show that $d(1) = 1$ by direct substitution of Eq. (D1). Then judicious application of the recurrence relation for U_{k+1} results in

$$\begin{aligned} d(k+1) &= U_{k+1}^2 - 2hU_{k+1}U_{k+1-1} + U_{k+1-1}^2 \\ &= (2hU_k - U_{k-1})^2 - 2h(2hU_k - U_{k-1})U_k + U_k^2 \\ &= (4h^2U_k^2 - 4hU_kU_{k-1} + U_{k-1}^2) - 2h(2hU_k^2 - U_kU_{k-1}) + U_k^2 \\ &= 4h^2U_k^2 - 4hU_kU_{k-1} + U_{k-1}^2 - 4h^2U_k^2 + 2hU_kU_{k-1} + U_k^2 \\ &= U_{k-1}^2 - 2hU_kU_{k-1} + U_k^2 \\ &= d(k) \end{aligned} \quad (\text{D3})$$

for any k . If $d(1) = 1$, and $d(k) = d(k+1)$ for all k , then

$d(k) = 1$ for all k , and the required identity is proven.

¹ H. Geiger and E. Marsden, *LXI, The laws of deflexion of α -particles through large angles*, The London, Edinburgh,

and Dublin Philosophical Magazine and Journal of Science,

- 25, 604-623 (1913).
- ² W. Kim, L. Covaci and F. Marsiglio, “Hidden symmetries of electronic transport in a disordered one-dimensional lattice,” *Phys. Rev. B* **73**, 195109-1-5 (2006).
 - ³ Wonkee Kim, L. Covaci, and F. Marsiglio, “Impurity scattering of wave packets on a lattice,” *Phys. Rev. B* **74**, 205120-1-9 (2006).
 - ⁴ An excellent discussion of this very issue can be found in T. Norsen, J. Lande and S.B. McKagan, “How and why to think about scattering in terms of wave packets instead of plane waves,” arXiv:0808.3566 (2008). Parts of this manuscript were published in T. Norsen, “The pilot-wave perspective on quantum scattering and tunnelling,” *Am. J. Phys.* **81**, 258-266 (2013).
 - ⁵ K. Schönhammer, “Unusual broadening of wave packets on lattices,” *Am. J. Phys.* **87**, 186-193 (2019).
 - ⁶ M. Staelens and F. Marsiglio, “Scattering problems via real-time wave packet scattering,” *Am. J. Phys.* **89**, 693-701 (2021).
 - ⁷ See, for example, <https://phet.colorado.edu/en/simulations/category/new>.
 - ⁸ Philip Phillips, *Advanced Solid State Physics*, (Westview Press, Boulder, CO, 2003).
 - ⁹ Peter Markoš and Costas M. Soukoulis, *Wave Propagation: From Electrons to Photonic Crystals and Left-Handed Materials*, (2nd ed. Princeton University Press, Princeton, 2008).
 - ¹⁰ John D. Joannopoulos, Steven G. Johnson, Joshua N. Winn and Robert D. Meade, *Photonic Crystals: Molding the Flow of Light*, (2nd ed. Princeton University Press, Princeton, 2008).
 - ¹¹ David J. Griffiths and Nicholas F. Taussig, “Scattering from a locally periodic potential,” *Am. J. Phys.* **60**, 883-888 (1992).
 - ¹² D.W.L. Sprung, Hua Wu and J. Martorell, “Scattering by a finite periodic potential,” *Am. J. Phys.* **61**, 1118-1124 (1993).
 - ¹³ David J. Griffiths and Carl A. Steinke, “Waves in locally periodic media,” *Am. J. Phys.* **69**, 137-154 (2001). See Ref. 13 in this paper for earlier references, each of which carried out some form of the same derivation in the continuum limit.
 - ¹⁴ F. Marsiglio, “The harmonic oscillator in quantum mechanics: A third way,” *Am. J. Phys.* **77**, 253-258 (2009).
 - ¹⁵ In fact there are many aspects of this problem that can be utilized in a course setting, particularly one that emphasizes topics in condensed matter physics. For example, the eigenvalues for such a problem, given analytically in Appendix B, indicate $E_{k_0} = 0$ for $k_0 a = \pi/2$, yet the wave packet moves, because it is the group velocity that plays the important role of governing the speed of the wave packet.
 - ¹⁶ D.H. Dunlap, H.-L. Wu and P.W. Phillips, “Absence of localization in a random-dimer model,” *Phys. Rev. Lett.* **65**, 88-91 (1990).
 - ¹⁷ H.-L. Wu and P.W. Phillips, “Polyaniline is a random-dimer model - a new transport mechanism for conducting polymers,” *Phys. Rev. Lett.* **66**, 1366-1369 (1991).
 - ¹⁸ H.-L. Wu, W. Goff and P.W. Phillips, “Insulator-metal transitions in random lattices containing symmetrical defects,” *Phys. Rev. B* **45**, 1623-1628 (1992).
 - ¹⁹ P. K. Datta, D. Giri, and K. Kundu, “Nonscattered states in a random-dimer model,” *Phys. Rev. B* **47**, 10727-10737 (1993).
 - ²⁰ D. Giri, P. K. Datta, and K. Kundu, “Tuning of resonances in the generalized random trimer model,” *Phys. Rev. B* **48**, 14113-14120 (1993).
 - ²¹ <https://mathworld.wolfram.com/UnimodularMatrix.html>.